# NUMERICAL EXPLORATION OF STAGED HYDROGEN COMBUSTION IN A STRUT BASED SCRAMJET COMBUSTOR

Soumyajit Saha and Debasis Chakraborty
Directorate of Computational Dynamics
Defence Research and Development Laboratory (DRDL)
Kanchanbagh Post, Hyderabad-500 058
Email : debasis_cfd@drdl.drdo.in/debasis_drdl@yahoo.co.in

**Abstract**

*Scramjet combustor with fuel injection from strut and wall is numerically simulated using three-dimensional Navier Stokes equations along with k - ε turbulence model. Turbulence - chemistry interaction is modeled through Eddy Dissipation Concept (EDC) based on infinitely fast rate kinetics. The simulations captured all the essential features of flow field for various combinations of fuel injections from the strut and the wall. The computed surface pressures match very well with the experimental values for both reacting and non-reacting cases. Performance parameters are evaluated from the computed flow variables. It was found that more fuel could be injected in the scramjet combustor through staged injection without inlet - combustor interaction.*

## Introduction

The success of efficient design of a hypersonic air-breathing cruise vehicle largely depends on the proper choice of propulsion system. This type of vehicle, according to current proposals, would use scramjet propulsion system with hydrogen fuel. A vital part of the effort to develop the scramjet combustor is the ability to understand the mixing and combustion process inside the combustor.

Experimental and numerical results [1,2] show that fuel injection from wall will result in reaction zones that occupy only a small fraction of the flow field. Therefore, not all of the oxygen supplied by the air stream entering into the combustor can participate in the heat release process. Furthermore, the reaction zones close to the wall will exert excessive thermal loads on the structure of the combustor. This problem of slow lateral fuel transport in the air stream can be circumvented by injecting the fuel in the core region of the flow by means of struts / pylon. Fuel injection from the struts has been experimented upon in some subscale scramjet engine including airframe integrated scramjet module [3,4]. The subscale scramjet engine being developed at NAL, Japan [5], uses the fuel injection strut to improve mixing. Scramjet engines with struts were tested at Ramjet Engine Test facility for Mach 4, 6 and 8 conditions [6-8]. A number of experimental and numerical studies [9-16] were reported in the literature to focus on various aspects of drag losses, mixing, combustion, intake - combustor interactions etc. Masuya et al. [6] studied the ignition and combustion performance of a scramjet combustor with Mach 2.5 vitiated air. Five strut models with various leading edge geometries were tested without fuel injection to select the less flow-disturbing configuration. Non-reactive flow simulations were also conducted using 2D Navier Stokes equations. It was found that non-reactive flow field was sensitive to the leading edge geometry of the strut and the relative position between the reflected shock wave impingement and rearward step of the strut was a critical parameter. Using the selected strut configuration, combustion and ignition tests were conducted [6]. It was observed that mixing and combustion with less flow-disturbing strut was considerably worse than those with a more flow-disturbing strut. Fuel from the strut ignited at a lower air temp than that from the wall in both the auto ignition and forced ignition. Mitani et al. [10] simulated the nonreacting flow field of the Scramjet engine with strut using a three-dimensional N-S solver with unstructured grid. An upwind finite volume scheme for arbitrary shaped cell [17] is used for the solution algorithm. The internal drag of the engine estimated from the calculated pressure distribution was found to be one third of the total drag. Mitani et al. [11] studied

**Paper Code : V63 N4/732-2011**. Manuscript received on 18 Oct 2010. Reviewed and accepted as a Full Length Contributed Paper on 29 Jul 2011

the reaction and mixing-controlled combustion in Scramjet engine with strut injection from the gas sampling from the combustor exit for Mach 4 to Mach 8 test condition. The correlation between the fuel equivalence ratio and combustion efficiency indicate that there is a shift of the reaction-controlled combustion for Mach 4 condition to the mixing-controlled combustion in Mach 8 condition. Gerlinger et al. [12] carried out nonreacting simulation of $H_2$/air mixing process in a Scramjet Combustor with planar and lobed strut injectors. Three-dimensional N-S equations with K-ω turbulence model were solved using an implicit lower-upper symmetric Gauss-Seidel algorithm [18]. Comparisons of performance parameters between planar and lobed strut injectors show that the mixing is better for lobed injectors because of generation of streamwise vortices.

Injection of more fuel from the strut can cause considerable inlet-combustor interaction that may lead to engine unstart condition and more fuel injection from wall will cause lesser penetration and the reaction zone will contain only a small portion of the combustor close to the wall. To reduce inlet-combustor interaction and to have better mixing and combustion, idea of staged combustion has been introduced [19] and a multi-injection port configuration has been adopted in some combustor models [20]. A staged supersonic combustor with a strut for the first stage injection and second-stage wall injection at its divergent section was experimentally investigated by Tomioka et al. [13, 14] in a direct-connect wind tunnel facility. Various injection schemes were chosen by changing the equivalence ratios and the injection locations so that the combustor inlet interaction is minimized. The performance of the combustor is evaluated at both fuel rich and fuel lean conditions. The combustor tests were carried out for the combustor entry Mach number of 2.5, total temperature of 1500 K and total pressure of 1.0 MPa, which are almost the combustor entrance condition under Mach 6 flight condition. Sonic hydrogen was injected from the strut and the wall with various equivalence ratios. Though, the $H_2$ injection from the strut for equivalence ratio 0.5 resulted in combustor-inlet interaction, a fuel flow rate greater than unity in equivalence ratio could be injected without occurrence of the interaction with the staged injection.

Numerical simulation are carried out in the present work for the staged scramjet combustor experiment of Tomioka et al. [13,14] for various fuel equivalence ratio from the strut and the wall. Three dimensional N-S equations are solved alongwith k-ε turbulence model and fast rate kinetics using commercial CFD software CFX [21]. Four different nonreacting and reacting cases (with different equivalence ratios) were considered to study the effect of staged fuel injection on combustor performance as well as combustor - inlet interaction problem in a hydrogen fuelled scramjet combustor. The computed results are compared with the experimental values and performance parameters were estimated from the computed flow variables.

## Experimental Condition [13, 14] for Which the Computation are Carried-out

The experiments for which the computations are carried out are a staged scramjet combustor in blowdown type wind tunnel facility [13,14]. The vitiated air heater was used to obtain high enthalpy airflow with a total temperature of $1500 \pm 50$ K. Oxygen was added to attain oxygen mole concentration of the test gas equal to that of standard air. Total pressure of the test gas flow was $1.0 \pm 0.03$ MPa. The test gas was accelerated through a contoured facility nozzle to Mach 2.5. The schematic diagram of the combustor is shown in Fig.1. The rectangular combustor was directly connected to a test facility nozzle. Between the facility nozzle and the combustor, a constant cross sectional area isolator with 239 mm length was installed. There was a backward facing step (2 mm height) on each sidewall at the exit of the isolator. A constant cross sectional area (56 mm in length) was attached downstream of the step. A strut with blunt leading edge (1 mm in radius) and a compression part (43.8 mm) with half wedge angle of $6^0$, 2 mm backward facing step on both sides on 28 mm straight portion is installed in the constant area section for fuel injection. Downstream of the constant area section, the sidewall diverged at an angle of $3.1^0$ for 600 mm. Three sets of injectors (2.5 mm diameter, 4 on each side wall in each set) were installed at 176 mm, 296 mm and 416 mm downstream of the step respectively. Tests were carried out with various fuel equivalence ratios through different set of injectors. In all the cases, gaseous hydrogen at room temperature was injected at sonic speed.

## The Code and Computational Detail

### Governing Equation

The appropriate system of equations governs the turbulent compressible gas may be written as

Continuity equation:

$$\frac{\partial \rho}{\partial t} + \frac{\partial}{\partial x_k}(\rho u_k) = 0 \quad k = 1, 2, 3$$

Momentum equation :

$$\frac{\partial}{\partial t}(\rho u_i) + \frac{\partial}{\partial x_k}(\rho u_i u_k) + \frac{\partial p}{\partial x_i} = \frac{\partial(\tau_{ik})}{\partial x_i}, \quad i, k = 1, 2, 3$$

Energy equation :

$$\frac{\partial}{\partial t}(\rho H) + \frac{\partial}{\partial x_k}(\rho u_k H) = -\frac{\partial}{\partial x_k}(u_j \tau_{jk}) + \frac{\partial q}{\partial x_k}, \quad j, k = 1, 2, 3$$

Turbulent kinetic energy ($k$) equation :

$$\frac{\partial}{\partial t}(\rho k) + \frac{\partial}{\partial x_k}(\rho u_k k) = \frac{\partial}{\partial x_k}\left(\left(\frac{\mu_l}{\mathrm{Pr}} + \frac{\mu_t}{\sigma_k}\right)\frac{\partial k}{\partial x_k}\right) + S_k$$

Rate of dissipation of turbulent kinetic energy (ε) equation:

$$\frac{\partial}{\partial t}(\rho \varepsilon) + \frac{\partial}{\partial x_k}(\rho u_k \varepsilon) = \frac{\partial}{\partial x_k}\left(\left(\frac{\mu_l}{\mathrm{Pr}} + \frac{\mu_t}{\sigma_\varepsilon}\right)\frac{\partial \varepsilon}{\partial x_k}\right) + S_\varepsilon$$

Species mass fraction (z) :

$$\frac{\partial}{\partial t}(\rho z) + \frac{\partial}{\partial x_k}(\rho u_k z) = \frac{\partial}{\partial x_k}\left(\left(\frac{\mu_l}{\mathrm{Pr}} + \frac{\mu_t}{\sigma_c}\right)\frac{\partial z}{\partial x_k}\right)$$

Where, $\rho$, $u_i$, $p$, $H$ are the density, velocity components, pressure and total energy respectively and $\mu = \mu_l + \mu_t$ is the total viscosity; $\mu_l$, $\mu_t$ being the laminar and turbulent viscosity and $Pr$ is the Prandtl number. The source term $S_k$ and $S_\varepsilon$ of the $k$ and ε equation are defined as

$$S_k = \tau_{ik}\frac{\partial u_i}{\partial x_k} - \rho\varepsilon \text{ and } S_\varepsilon = C_{\varepsilon 1}\tau_{ik}\frac{\partial u_i}{\partial x_k} - C_{\varepsilon 2}\frac{\rho \varepsilon^2}{k}$$

where turbulent shear stress is defined as

$$\tau_{ik} = \mu_t\left(\frac{\partial u_i}{\partial x_k} + \frac{\partial u_k}{\partial x_i}\right)$$

Laminar viscosity ($\mu_l$) is calculated from Sutherland law as

$$\mu_l = \mu_{ref}\left(\frac{T}{T_{ref}}\right)^{3/2}\left(\frac{T_{ref}+S}{T+S}\right)$$

where, $T$ is the temperature and $\mu_{ref}$, $T_{ref}$ and $S$ are known coefficient. The turbulent viscosity $\mu_t$ is calculated as

$$\mu_t = c_\mu \frac{\rho k^2}{\varepsilon}$$

The coefficients involving in the calculation of $\mu_t$ are taken as

$$c_\mu = 0.09, \quad C_{\varepsilon 1} = 1.44, \quad C_{\varepsilon 2} = 1.92$$

$$\sigma_\kappa = 1.0, \quad \sigma_\varepsilon = 1.3, \quad \sigma_c = 0.9$$

The heat flux $q_k$ is calculated as $q_k = -\lambda\frac{\partial T}{\partial x_k}$, $\lambda$ is the thermal conductivity.

**Combustion Modeling**

For combustion, the eddy dissipation combustion model is used for its simplicity and robust performance in predicting reactive flows. The eddy dissipation model is based on the concept that chemical reaction is fast relative to the transport process in the flow and when reactants mix at the molecular level they instantaneously form products. The model assumes that the reaction rate may be related directly to the time required to mix reactants at molecular level. In turbulent flows, this mixing time is dictated by the eddy properties and therefore the burning rate in proportional to the rate at which turbulent kinetic energy is dissipated i.e., reaction rate $\alpha$ ε/k, where k is the turbulent kinetic energy and ε is its rate of dissipation. The chemistry of the combustion reaction is represented on a molar basis by: $H_2 + 0.5O_2 = H_2O$.

**Discretisation of Governing Equations**

The CFX TASCflow solver utilizes a finite volume approach, in which the conservation equations in differential form are integrated over a control volume described around a node, to obtain an integral equation. The pressure integral terms in momentum integral equation and the spatial derivative terms in the integral equations are evaluated using finite element approach. An element is described with eight neighboring nodes. The advective term is evaluated using upwind differencing with physical advection correction. The set of discretised equations form a set of algebraic equations: $A\,\vec{x} = b$ where $\vec{x}$ is the

solution vector. The solver uses an iterative procedure to update an approximated $x_n$ (solution of $x$ at $n^{th}$ time level) by solving for an approximate correction $x'$ from the equation $A\ \vec{x}' = \vec{R}$, where $\vec{R} = \vec{b} - A\ \vec{x_n}$ is the residual at $n^{th}$ time level. The equation $A\ \vec{x}' = \vec{R}$ is solved approximately using an approach called Incomplete Lower Upper factorization method. An algebraic multigrid method is implemented to reduce low frequency errors in the solution of the algebraic equations. Maximum residual $(= \phi_j^{n+1} - f(\phi_j^{n+1}, \phi_j^n)) < 10^{-5}$ is taken as convergence criteria.

## Results and Discussions

Taking the advantage of two plane of symmetry, only one - fourth of the geometry is simulated. A total of 0.17 million grid points were used for the numerical simulation. The grid was finer near the strut, walls and the step. In the rest of the region the grid was relatively coarse. The schematic of the grid in the plane of symmetry is shown in Fig.2. Also, shown in the figure, the blown up view of the grid distribution near the fuel injection. The grid independence of the results were demonstrated by comparing the results with two different grids (presented later). The vitiated air consisted of 0.23 of $O_2$, 0.111 of $H_2O$, and remaining 0.679 of $N_2$ by mass fraction. $H_2$ was injected at sonic speeds, and at a total temperature of 300 K into the combustor. The injection plane pressure was adjusted to achieve desired equivalence ratio. Four different simulations were carried out for various nonreacting and reacting cases corresponding to experimental conditions which encompass both fuel rich and fuel lean conditions.

- Non reacting case without fuel injections
- Reacting case with fuel injection only from strut ($\varphi_1$=0.34)
- Reacting case with fuel injection both from strut ($\varphi_1$=0.35) and wall ($\varphi_2$=0.44)
- Reacting case with fuel injection from strut ($\varphi_1$ = 0. 35) and the wall ($\varphi_2$=0.90)

### Non Reacting Flow Analysis Without Fuel Injection

To understand the general feature of the flow field without injection (pressure, temperature and Mach number distribution), nonreacting simulation is first carried out. The Mach number and pressure distribution in the symmetry plane of the combustor is presented in Figs.3 and 4 respectively for the case without fuel injection. The blown up view of flow field near the strut region is also shown in the figure to depict the flow structure clearly. The flow field in the combustor is supersonic. The shock form the leading edge of the strut hits the upper wall increasing the wall pressure. The complex shock interaction process in the combustor is clearly visible. The axial distribution of computed wall pressure for two different grids is compared with the experimental results in Fig.5. Pressure has been non-dimensionalised by total pressure $p_o$ and x = 0 is taken at the location of the step of the combustor. It can be noticed that by changing the grids from 0.17 million to 0.3 million has not changed the results appreciably thus demonstrating the grid independence of the results. A good agreement between the experiment and computation has been obtained. All the shock interaction in the combustor has been captured nicely in the computation. The sudden increase near x = 0 is due to the incidence of the strut leading edge shock at the wall and immediate decrease of surface pressure is due to the expansion at the strut step. A sharp increase at x = 50 mm is due to the reattachment shock on the strut and another steep decrease at x = 70 mm was caused by incident of reflected strut leading edge shock. The pressure rise at x = 90 mm was caused by incident of reflected strut leading edge shock. The pressure rise at the exit of the combustor (x > 400 mm) was due to separation of flow that is seen clearly in the blown up view of the velocity vector near the exit of the combustor in Fig.6.

### Reacting Computation with Fuel Injection only from Strut ($\varphi_1$= 0.34)

The Mach number and pressure distributions in the symmetry plane of the combustor are presented in Fig.7. Comparing these results with that of non-reacting case, we can notice drastic changes in the flow structure. The expansion wave near the step for the non-reacting case is cancelled due to heat release and generation of compression waves. The Mach number near the central portion of the combustor, where the reaction occurs, reduces significantly. The simulation has also captured the bow shock near the injection strut crisply. The temperature and water mass fraction distribution in the combustor are shown in Fig.8. It is clear from the figure that the reaction occurs only in the central zone of the combustor. The flow field in the rest of the combustor almost remains unreacted. The surface pressure comparison between the experiment and computation is presented in Fig.9. A very good match is observed except near the fuel injection location, where the computation over predicted the surface pressure. This

difference may be due to the use of fast chemistry, which caused instantaneous heat release in the modeling resulting in prediction of high surface pressure.

### Reacting Computation with Fuel Injection from Strut and Wall (φ1+φ2=0.35+0.44)

Computations were carried out with hydrogen injection from both strut and wall. Hydrogen with equivalence ratio 0.35 is injected from the strut at x = 0 and hydrogen with equivalence ratio 0.44 is injected from the divergent portion of the combustor at the distance of 296 mm from the strut injection point. The water mass fraction and oxygen mass fraction distribution is shown in Fig.10. The higher water mass fraction zones (lower oxygen mass fraction zones) mark the region where the reaction occurs. The reaction zone for the strut injection is confined at the center and the zone for the wall injection is confined near the wall. The comparison of the surface pressure between the experiment and computations are shown in Fig.11. A good overall match is observed. As in the previous case, the computation over predicted the first peak near the strut injection while the computation could properly predict the second peak. The surface pressure in the divergent part is slightly underpredicted. It can also be noted that the wall injection has not changed the pressure pattern in the strut injection location although higher pressure is noticed about 100 mm upstream of the wall injection. This demonstrates the usefulness of staggered injection in injecting more fuel in the scramjet combustion chamber.

### Reacting Computation for Fuel Rich Case with Fuel Injection from Strut and Wall (φ1+φ2=0.35+0.90)

Finally, the computations were carried out for the case of fuel rich condition where $H_2$ with equivalence ratio of 0.35 is injected from the strut and hydrogen with equivalence ratio 0.9 is injected at the divergent portion in the combustor at a distance of 296 mm from the first injection location. The Mach number and pressure distribution in the symmetry plane for this case is shown in Fig.12. The water mass fraction and the oxygen mass fraction distribution are presented in Fig.13 indicating the regions of reaction. The cross sectional view of oxygen mass fractions at various axial stations is presented in Fig.14. It is found that near the exit of combustor the intensive reaction is confined to the upper wall, which causes total depletion of oxygen. The surface pressure comparison between the experiment and computation is shown in Fig.15. A good overall match has been obtained. The fluctuations in wall pressure data are due to the repeated reflection of shock in the combustor. Pressure measurements at much finer interval in $0.15 < x < 0.3$ may be required to capture the shock reflections in the combustor. The pressure rise created by the second stage injection is seen to travel about 150 mm upstream but still did not affect the first stage injection from the strut.

The surface pressures for all the four cases are compared in Fig.16. With the second stage injection there is considerable increase in pressure in the divergent section, which is very necessary to increase the thrust. For the case of injection from strut and wall ($\varphi_1+\varphi_2$=0.35+0.44), there is no influence of the second stage injection in the first stage, while for the fuel rich case ($\varphi_1+\varphi_2$=0.35+0.90), the influence of wall injection has felt slightly upstream but it did not affect the pressure peak caused due to the strut injection. The water mass fraction distributions at the outlet of the combustor for the three reacting cases are shown in Fig.17. With the increase of $H_2$ mass flow rate, more water is formed at the outlet. This feature is also noticed in the axial distribution of area-averaged $Y_{h2o}$ in Fig.18. The axial distribution of combustion efficiencies for the three reaction cases is presented in Fig.19. The combustion efficiencies are calculated from the ratio of the achieved water mass fraction to the maximum possible water mass fraction what could have been formed due to reaction. For the injection case from the strut alone, the combustion efficiency is 100%. With additional injection of hydrogen from the wall in the divergent portion, some amount of hydrogen remains unburned and reduces the combustion efficiency. The simulations provide useful insight for deciding the fuel injection pattern to obtain good performance without any inlet-combustor interaction.

## Conclusions

A staged supersonic combustor with strut for first stage injection and second stage wall injection in the divergent portion is simulated numerically using a three dimensional Navier stokes equations along with k - ε model of turbulence. Combustion is modeled through a fast rate chemical kinetics. Simulation captures all the essential features of the flow field. Computed wall pressures match extremely well with the experimental values for the non-reacting cases. For the reacting cases, although a good overall match is obtained, computation over predicts the pressure rise due to first stage injection. The use of fast chemical kinetics may be the cause of this discrepancy. The second stage injection in the divergent section has increased the pressure considerably, which is highly desirable for the

scramjet design. The second stage injection has not altered the pressure field of the first stage injection. Thus, more fuel can be injected in the Scramjet Combustor through staged injection without any unfavorable combustor - inlet interaction. The second stage fuel had lower combustion efficiency due to the lesser degree of fine scale mixing than that in the first stage injection. The simulations provide useful guideline for injection pattern to avoid combustor inlet interaction in practical scramjet combustor.

**References**


1. Abbilt, J.D., Hartfiled, R.J. and Mc Daniel, J.C., "Mole Fraction Imaging of Transverse Injection in a Ducted Supersonic Flow", AIAA Journal, Vol.29, No.3, p.431, 1991.

2. Yokota, K. and Kaji, S., "Two and Three Dimensional Study on Supersonic Flow and Mixing Fields with Hydrogen Injection", AIAA paper No.95-6024, 1995.

3. Waltrup, P.J., Anderson, G.Y. and Stull, F.D.,"Supersonic Combustion Ramjet (Scramjet) Engine Development in the United States", Proceeding of the Third International Symposium on Air Breathing Engines, 1974, pp.835-861.

4. Northam, G.B. and Anderson, G.Y., "Supersonic Combustion Ramjet Research at Langley", AIAA paper No.86-0159, 1986.

5. Miyajima, H., Chinzei, N., Mitani, T., Wakamatser, Y. and Maita, M., "Development Status of the NAL Ramjet Engine Test Facility and Subscale Scramjet Engine", AIAA paper 92-5094, 1992.

6. Sunami, T., Sakuranaka, N., Tani, K., Kiraiwa, T. and Shimura, T., "Mach 4 Test of a Scramjet Engine - Effect of Isolator", Proceeding of 13$^{th}$ International Symposium of Air Breathing Engine, AIAA, Washington D.C, pp. 615-625, 1997.

7. Kanda, T., Hiraiwa, T., Mitani, T., Tomioka, S. and Chinzei, N., "Mach 6 Testing of a Scramjet Engine Model Journal of Propulsion and Power", Vol.13, No.4, pp.543-551, 1997.

8. Kanda, T., Sunami, T., Tomioka, S., Tani, K. and Mitani, T., "Mach 8 Testing of Scramjet Engine Model", Journal of Propulsion and Power, Vol.17, No.1, pp.132-138, 2001.

9. Masuya, G., Komuro, T., Murakami, A., Shinozaki, N., Nakamura, A., Murayama, M. and Ohwaki, K., "Ignition and Combustion Performance of Scramjet Combustor with Fuel Injection Struts", Journal of Propulsion and Power, Vol.11, No.2, pp.301-307, 1995.

10. Mitani, T., Kanda, T., Hiraiwa, T., Igarashi, Y. and Nakahashi, T., "Drags in Scramjet Engine Testing - Experimental and Computational Fluid Dynamics Studies", Journal of Propulsion and Power, Vol.15, No.4, pp.578-583, 1999.

11. Mitani, T., Chinzei, N. and Kanda, T., "Reaction and Mixing-Controlled Combustion in Scramjet Engines", Journal of Propulsion and Power, Vol.17, No.2, pp.308-313, 2001.

12. Gerlinger, P., Kasal, P., Stoll, P. and Bruggemann, D., "Experimental and Theoretical Investigation on 2D and 3D Parallel Hydrogen/Air Mixing in a Supersonic Flow", ISABE paper No. 2001-1019, 2001.

13. Tomioka, S., Murakami, A., Kudo, K. and Mitani, T., "Combustion Tests of a Staged Supersonic Combustor with a Strut", Journal of Propulsion and Power, Vol.17, No.2, pp.293-300, 2001.

14. Tomioka, S., Kobayashi, K., Kudo, K., Murakam, A. and Mitani, T., "Effects of Injection Configuration on Performance of a Stage Supersonic Combustor" Journal of Propulsion and Power, Vol.19, No.5, pp.876-884, 2003.

15. Glawe, D.D., Saminy, M., Nejad, A.S. and Cheng, T.H., "Effects of Nozzle Geometry on Parallel Injection from Base of an Extended Strut into a Supersonic Flow", AIAA paper No.95-0522, 1995.

16. Wepler Ulrich and Kaschel, W.W. ,"Numerical Investigation of Turbulent Reacting Flows in a Scramjet Combustor Model" AIAA paper No. 2002-3572, 2002.

17. Sharov, D. and Nkahashi, K., "Reordering of 3D Hybrid Unstructured Grids for Lower-Upper Sym-

metric Gauss-Seidel Computation", AIAA Journal, Vol.36, No.3, pp.484-486, 1998.

18. Gerlinger, P. and Bluggemann, D., "An Implicit Multigrid Scheme for the Compressible Navier-stokers Equation with Low Reynolds-Turbulence Closure", Journal of Fluids Engineering, Vol.120, pp.257-262, 1998.

19. Billig, F.S., "Combustion Process in Supersonic Flow", Journal of Propulsion and Power, Vol.4, No.3, pp.209-216, 1988.

20. Vinogradov, V., Grachu, V., Petrov, M. and Sheet, J., "Experimental Investigation of 2D Dual Mode Scramjet with Hydrogen Fuel at Mach 4-6", AIAA paper No. 90-5269, 1990.

21. CFX Computational Fluid Dynamics Software, Version 5.6, CFX-ANSYS Software Ltd, 2004.

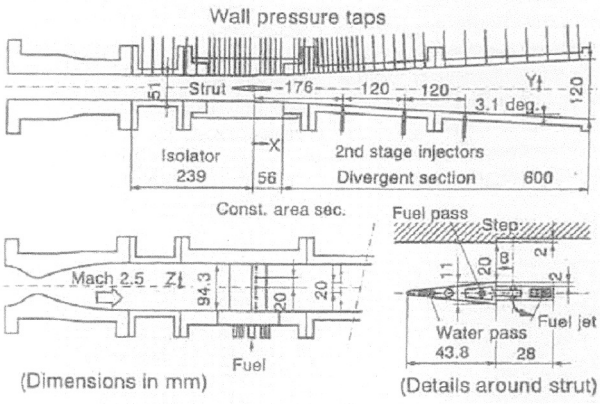


*Fig.1 Schematic of the Combustor with the Strut*

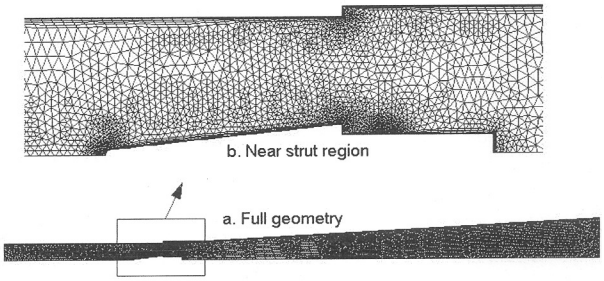


*Fig.2 Grid Distribution in the Symmetry Plane (a) Full Geometry, (b) Near Strut Region*

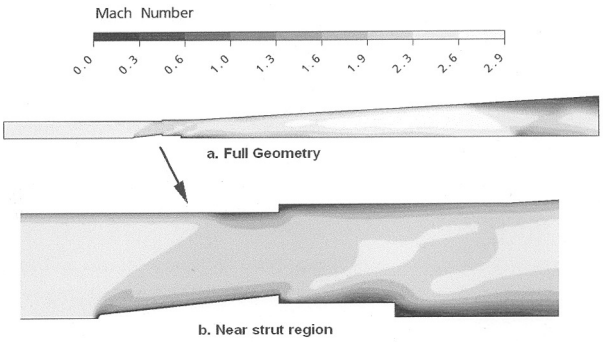


*Fig.3 Mach Number Distribution in the Symmetry Plane for Non Reacting Case (a) Full Geometry, (b) Near Strut Region*

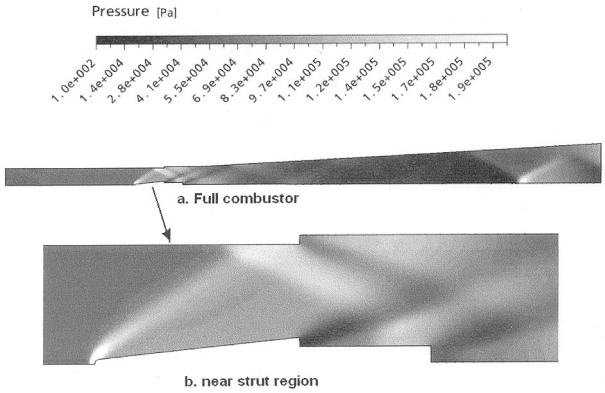


*Fig.4 Pressure Distribution in the Symmetry Plane for Non Reacting Case (a) Full Geometry, (b) Near Strut Region*

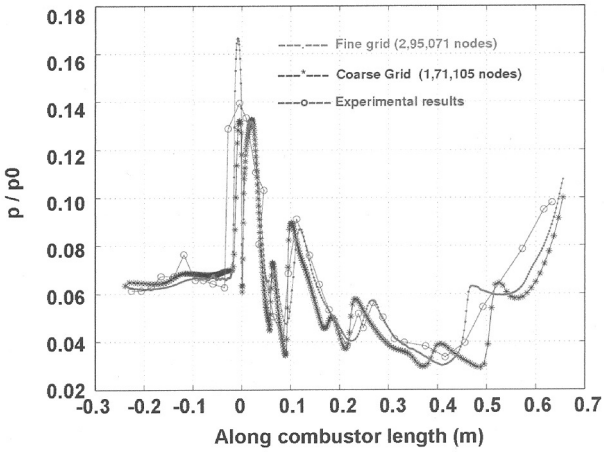


*Fig.5 Comparison of Wall Pressure Distribution for Non Reacting Case*

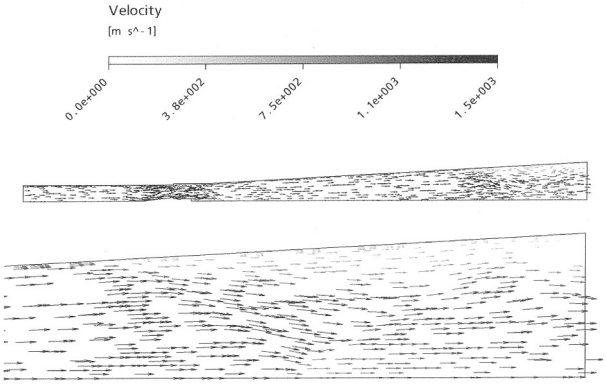


*Fig.6 Blown up View of Velocity Vector Near the Exit of the Combustor*

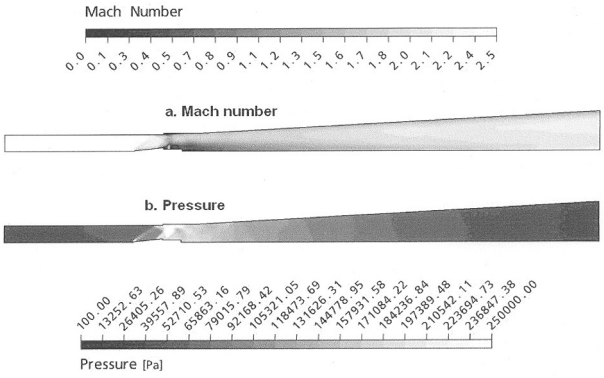


*Fig.7 Flow Variables in the Symmetry Plane for Reacting Case with Strut Injection ($\varphi_1$=0.34) (a) Mach Number, (b) Pressure*

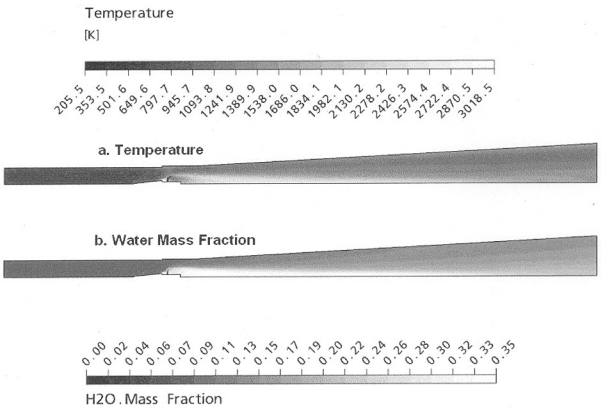


*Fig.8 Flow Variables in the Symmetry Plane for Reacting Case with Strut Injection ($\varphi_1$=0.34) (a) Temperature, (b) Water Mass Fraction*

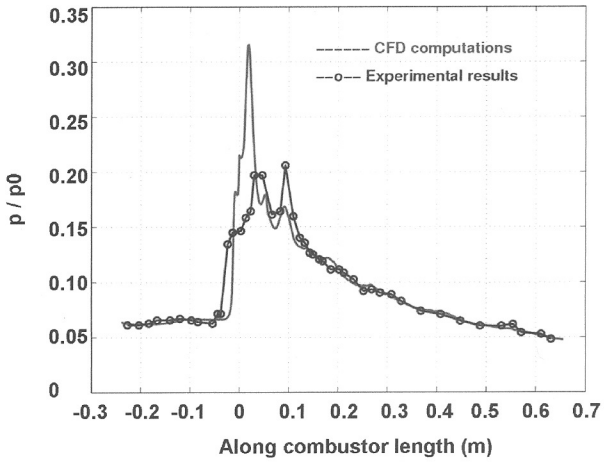


*Fig.9 Comparison of Wall Pressure Distribution for Reacting Case with Fuel Injection from Strut ($\varphi_1$=0.34)*

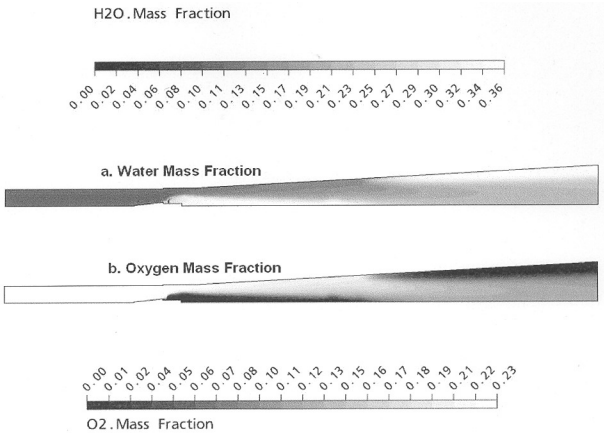


*Fig.10 (a) Water Mass Fraction, (b) Oxygen Mass Fraction Distribution at the Symmetry Plane for Fuel Injection from Strut and Wall ($\varphi_1$+$\varphi_2$=0.35+0.44)*

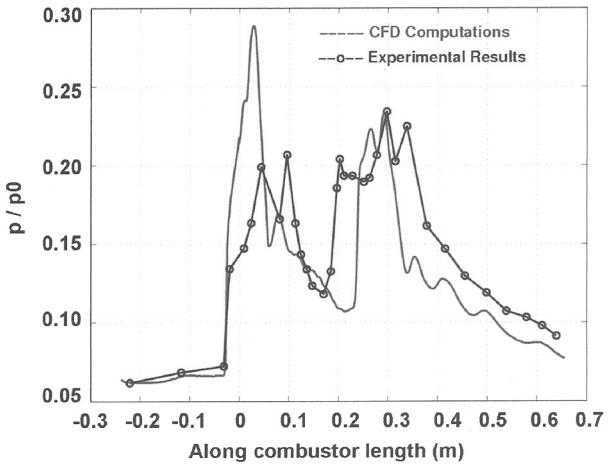


*Fig.11 Comparison of Wall Pressure Distribution for Reacting Case with Fuel Injection from Strut and Wall ($\varphi_1+\varphi_2=0.35+0.44$)*

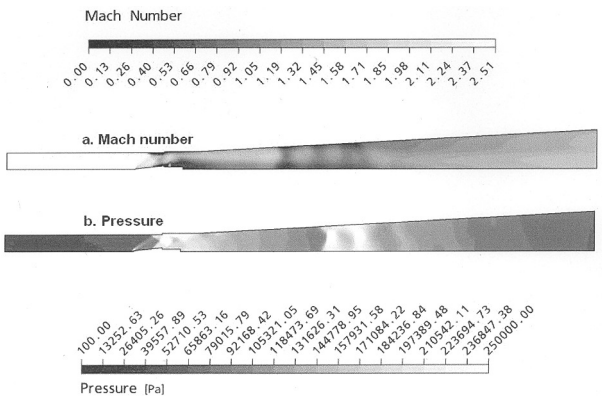


*Fig.12 Flow Variables in the Symmetry Plane for Reacting Case with Strut and Wall Injection ($\varphi_1+\varphi_2=0.35+0.90$) (a) Mach Number, (b) Pressure*

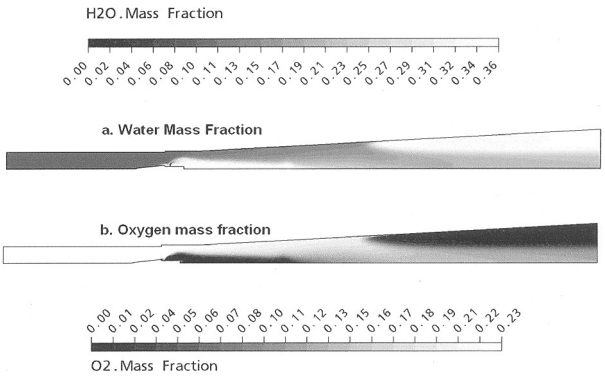


*Fig.13 Flow Variables in the Symmetry Plane for Reacting Case with Strut and Wall Injection ($\varphi_1+\varphi_2=0.35+0.90$) (a) Water Mass Fraction, (b) Oxygen Mass Fraction*

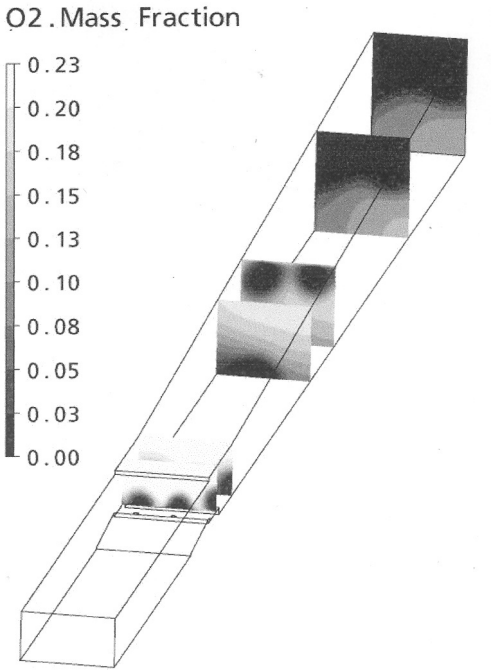


*Fig.14 Cross Sectional View of Oxygen Mass Fraction for Reacting Case with Strut and Wall Injection ($\varphi_1+\varphi_2=0.35+0.90$)*

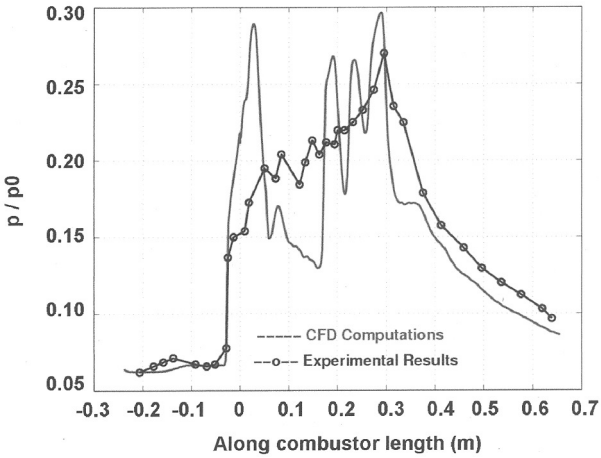


*Fig.15 Comparison of Wall Pressure Distribution for Reacting Case with Fuel Injection from Strut and Wall ($\varphi_1+\varphi_2=0.35+0.90$)*

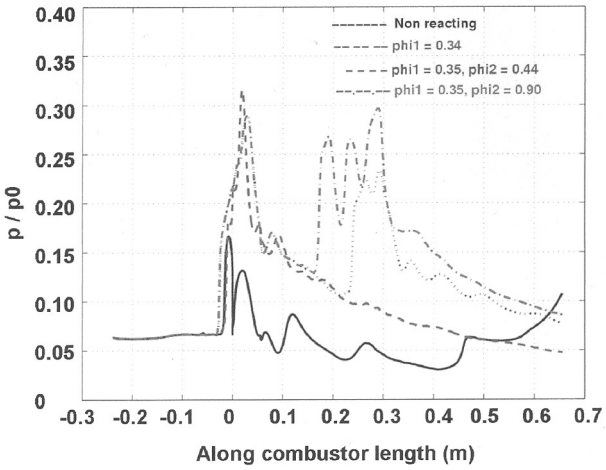


*Fig.16 Comparison of Wall Pressure Distribution for all Four Reacting and Non Reacting Cases*

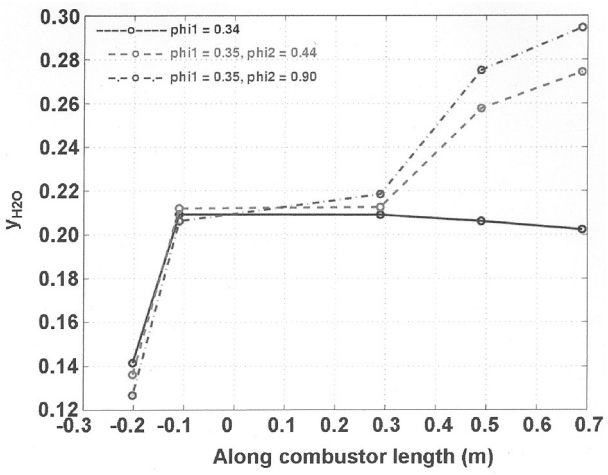


*Fig.18 Axial Distribution of Area Averaged Water Mass Fraction for the Reacting Cases*

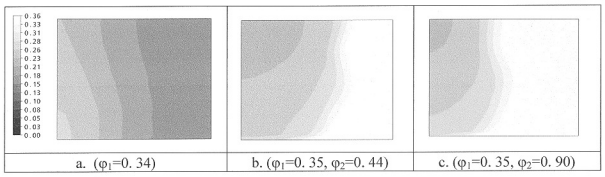


*Fig.17 Water Mass Fraction Distribution at the Outlet for the Reacting Cases, (a) $\varphi_1$=0.34, (b) $\varphi_1+\varphi_2$=0.35+0.44, (c) $\varphi_1+\varphi_2$=0.35+0.90*

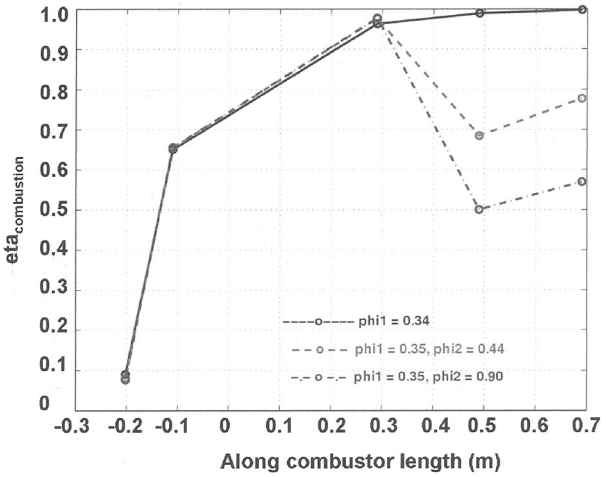


*Fig.19 Axial Distribution of Combustion Efficiency for the Reacting Cases*